Meteoritics & Planetary Science 41, Nr 2, 247–262 (2006)
Abstract available online at http://meteoritics.org

Shock re-equilibration of fluid inclusions in crystalline basement rocks from the Ries crater, Germany

Megan E. ELWOOD MADDEN[1†*], David A. KRING[2], and Robert J. BODNAR[1]

[1]Department of Geosciences, Virginia Polytechnic Institute, Blacksburg, Virginia 24060, USA
[2]Lunar and Planetary Laboratory, The University of Arizona, Tucson, Arizona 85721, USA
[†]Present address: Environmental Sciences Division, Oak Ridge National Laboratory, Oak Ridge, Tennessee 37831–6036, USA
[*]Corresponding author. E-mail: maddenme@ornl.gov

(Received 10 June 2005; revision accepted 22 August 2005)

Abstract–This study examines the effects of shock metamorphism on fluid inclusions in crystalline basement target rocks from the Ries crater, Germany. The occurrence of two-phase fluid inclusions decreases from shock stage 0 to shock stage 1, while single-phase inclusions increase, likely as a result of re-equilibration. In shock stages 2 and 3, both two-phase and single-phase inclusions decrease with increasing shock stage, indicating that fluid inclusion vesicles are destroyed due to plastic deformation and phase changes in the host minerals. However, quartz clasts entrained in shock stage 4 melts contain both single-phase and two-phase inclusions, demonstrating the rapid quenching of the melt and the heterogeneous nature of impact deformation. Inclusions in naturally shocked polycrystalline samples survive at higher shock pressures than those in single crystal shock experiments. However, fluid inclusions in both experimental and natural samples follow a similar trend in re-equilibration at low to moderate shock pressures leading to destruction of inclusion vesicles in higher shock stages. This suggests that shock processing may lead to the destruction of fluid inclusions in many planetary materials and likely contributed to shock devolatilization of early planetesimals.

INTRODUCTION

In recent years, much of the research and exploration in planetary science has focused on the distribution and role of volatiles in the evolution of the solar system. This research and exploration effort is driven by our search for environments where liquid water may have been (or is) active and therefore may have been (or still is) hospitable for life.

A series of orbiting spacecraft and robotic landers have been sent to Mars to search for evidence that liquid water was once active at or near the surface (Soffen 1976; Golombek et al. 1997; Feldman et al. 2002; Malin et al. 1998; Squyres et al. 2004; Bibring et al. 2005). Measurements made by the Galileo spacecraft indicate that a subsurface ocean may exist beneath Europa's icy crust (Carr et al. 1998) and the Cassini spacecraft is currently investigating the role of volatiles on Titan and Saturn's other moons (Porco et al. 2005). Observations of hydrous phases in interplanetary dust particles suggest that even primitive solar system materials contain water (Zolensky and Barrett 1993). In addition, a number of recent meteorite studies have demonstrated that volatiles, including water, have been active on some chondritic parent bodies (Fredriksson and Kerridge 1988; Keller et al. 1994; Endress et al. 1996). In addition, halides and carbonates in the Shergotty, Nakhla, and Chassigny (SNC) meteorites provide further evidence of aqueous processes on Mars (Bridges et al. 2001; Warren 1998).

These missions and laboratory studies provide ample evidence that water has been active throughout the solar system since its early stages. However, the only direct samples we have of extraterrestrial liquid water are in the form of rare fluid inclusions in meteorites. Fluid inclusions are nanoliter volumes of fluid trapped in minerals as they precipitate (Fig. 1) (Roedder 1984). These small droplets of fluid are a unique tool that can be used to directly analyze geochemically active fluids that have been trapped and stored in a host mineral for perhaps billions of years.

While fluid inclusions are nearly ubiquitous in terrestrial rocks that form in the presence of a fluid phase (water, CO_2, methane, igneous melt, etc. [Roedder 1984]), only a few confirmed observations of fluid inclusions in meteorites can be found in the literature (Bodnar 1999; Bridges et al. 2001; Rubin et al. 2002; Zolensky et al. 1999). However, many other meteorites contain aqueous alteration minerals that

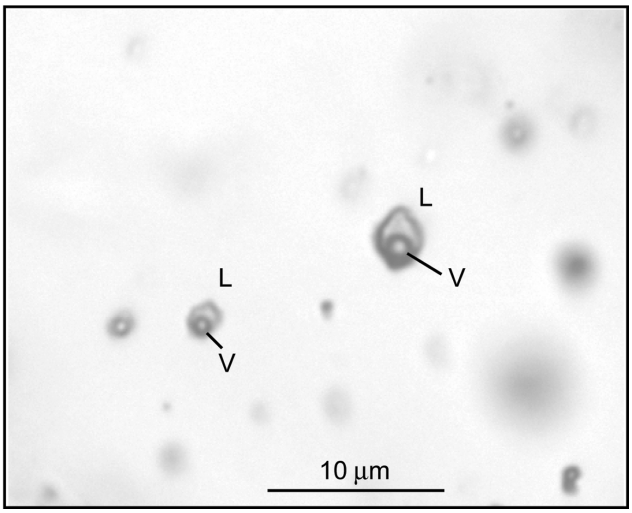

Fig. 1. Photomicrograph of quartz containing two-phase fluid inclusions in shock stage 0 sample (#719 from Stöffler [1971] collected at Wegenhausen) from the Ries impact crater. These aqueous fluid inclusions contain a liquid (*L*) and a vapor (*V*) phase.

demonstrate that water and other volatiles were active on the meteorite parent bodies, even though the samples contain no inclusions (Bridges et al. 2001; Endress et al. 1996; Fredriksson and Kerridge 1988).

If water was geochemically active on meteorite parent bodies, why don't we find fluid inclusions more commonly in meteorites? In some cases, fluid inclusions are trapped in highly soluble phases, such as the aqueous inclusions within halite in the Monahans and Zag H5 chondrites (Rubin et al. 2002; Zolensky et al. 1999). These fluid inclusions were only preserved because the meteorites did not encounter terrestrial water and were carefully processed in order to preserve the soluble phases. However, most fluid inclusions in terrestrial rocks are trapped in relatively insoluble carbonate and silicate phases. Therefore, we would also expect to find fluid inclusions in planetary carbonate and silicate phases, even if the more soluble phases have been destroyed. Alternatively, shock processing of planetary materials may cause previously trapped fluid inclusions to re-equilibrate, resulting in devolatilization of the target rock and the destruction of fluid inclusion features.

The results of a previous experimental study demonstrate that low to moderate impact pressures may destroy any fluid inclusions trapped in single crystal quartz (Elwood Madden et al. 2004). The goal of this study is to determine if fluid inclusions in polycrystalline rocks re-equilibrate in a similar manner resulting in a loss of fluid inclusions. If fluid inclusions in crystalline rocks are also destroyed by natural shock metamorphism at moderate shock pressures, this would suggest that fluid inclusions may have formed on meteorite parent bodies, but were later destroyed due to impact processing, resulting in the relative scarcity of fluid inclusions observed in planetary materials (Zolensky et al. 1999). The polycrystalline rocks studied here may be most useful as terrestrial analogs for achondritic parent bodies.

By comparing the effect of natural shock metamorphism on fluid inclusions in polycrystalline samples, we will also evaluate whether the results of single crystal experiments can be applied to shock re-equilibration of fluid inclusions in natural impactites and shock metamorphosed planetary materials.

BACKGROUND INFORMATION

Fluid Inclusions in Impactites

Most previous studies of fluid inclusions in terrestrial impactites have focused on fluid inclusion assemblages trapped post-impact as a result of hydrothermal activity (Koeberl et al. 1989; Andersen and Burke 1996; Sturkell et al. 1998; Kirsimae et al. 2002; Hode et al. 2003; Lueders and Rickers 2004) or annealing of planar fractures and shock lamellae (Grieve et al. 1996; Whitehead et al. 2002). We are aware of only one previous study that examined the effect of shock metamorphism on fluid inclusions trapped in target rocks prior to a natural impact event (Komor et al. 1988). In their study, Komor et al. (1988) describe dark inclusions within the shock metamorphosed samples from the Siljan ring structure and interpret them to be fluid inclusions that have decrepitated due to heating associated with the impact event. However, because these features resemble inclusions that collapsed in static laboratory experiments (Vityk and Bodnar 1995), Elwood Madden et al. (2004) attribute similar features from single crystal quartz experiments to fluid inclusion collapse.

Shock Re-Equilibration

Previous experimental work (Elwood Madden et al. 2004) has demonstrated that shock metamorphism at low to moderate pressures (5–12 GPa) results in changes in fluid inclusion properties (re-equilibration) and the destruction of fluid inclusion features at moderate to high shock pressures (>12 GPa, 22). Fluid inclusion re-equilibration occurs when the fluid pressure within an inclusion differs from the confining pressure applied to the host mineral, resulting in a pressure gradient (Bodnar 2003; Vityk and Bodnar 1995). While the external pressure on the host mineral is determined by the lithostatic or hydrostatic load applied to the host mineral or by stress during shock loading, the pressure within fluid inclusions is determined by the pressure-vapor-temperature (*P-V-T*) properties of the enclosed fluid (Fig. 3). Therefore, the internal pressure within a fluid inclusion as determined by the temperature of the host mineral and the corresponding pressure along the liquid vapor curve or fluid isochore may differ greatly from the external pressure applied to the host mineral.

If the external pressure-temperature (*P*-*T*) path applied to the host rock closely follows the fluid isochore, then the external confining pressure on the host mineral and the internal fluid pressure will remain the same, resulting in no pressure gradient. In such cases, fluid inclusion re-equilibration will not occur and fluid inclusions will maintain their original volume and fluid density. However, if the external pressure applied to the host mineral exceeds the fluid pressure within the inclusions (path 1 in Fig. 3, where the external pressure [A] is greater than the internal pressure [B] along the fluid isochore), fluid inclusions may collapse due to the internal underpressure resulting in smaller inclusion volumes and therefore higher fluid densities (isochore A), smaller vapor bubbles, and lower homogenization temperatures (T_{hA}). Alternatively, if the fluid pressure within the inclusion is significantly greater than the pressure applied to the host mineral (path 2 in Fig. 3, where the internal pressure [B] is greater than the external pressure [C]), then the fluid inclusion vesicle may expand due to the internal overpressure resulting in a larger inclusion volume, lower fluid density (isochore C), larger vapor bubbles, and higher homogenization temperatures (T_{hC}). Therefore, by comparing fluid isochores to metamorphic pressure-temperature-time (*P*-*T*-*t*) paths, the likelihood and nature of fluid inclusion re-equilibration can be predicted.

During experimental and natural impact events, the target rocks experience rapid compression and unloading (Grieve et al. 1996) and experience significant heating due to entropy gains (Langenhorst 1994). The target rocks may experience elevated pressure conditions over a period of a few microseconds in impact experiments to tens of seconds in extremely large natural impact events. However, the waste heat remaining after adiabatic release will take much longer to dissipate, leaving the rocks at elevated temperature and ambient pressure for long periods of time (Gratz et al. 1992). Due to the shock *P*-*T*-*t* path, fluid inclusions in the target rock may experience significant external overpressures during the period of shock loading and compression which may result in the collapse of fluid inclusion vesicles (Fig. 4). However, this is followed by a period of internal overpressures once the target rocks return to ambient pressure but maintain an elevated temperature. This can lead to stretching of fluid inclusions and possibly decrepitation (complete loss of fluid along fractures) (Vityk et al. 2000; Elwood Madden et al. 2004).

The results of this previous experimental study suggest that fluid inclusions follow a systematic re-equilibration progression with increasing shock pressure (Fig. 2). At shock pressures of 5–6 GPa, homogenization temperatures increase due to fluid inclusion stretching. This suggests that the early high-pressure part of the *P*-*T*-*t* path (which causes the inclusion volume to decrease) has been overprinted by stretching, which occurs after the pressure has returned to ambient conditions but the rocks remain heated. At slightly higher pressures (6–8 GPa), decrepitated fluid inclusions are also observed. Between 6 and 12 GPa, fluid inclusions also collapse due to internal underpressure, and above 12 GPa, no evidence of previous fluid inclusions was found in single crystal quartz. These results suggest that below the Hugenoit elastic limit (HEL) of quartz, fluid inclusions re-equilibrate, leading to decrepitation and/or collapse of fluid inclusion vesicles. Above the HEL, fluid inclusion vesicles and all evidence of previous fluid inclusions are destroyed by plastic deformation and possibly phase transitions within the host mineral (Elwood Madden et al. 2004). The present study builds on these observations in two ways: first, by examining polymineralic nonporous, igneous and metamorphic rocks containing quartz, and second, by employing rocks from a natural impact event of substantially longer shock pulse duration approaching 1 second (Stöffler et al. 2002).

MATERIALS AND METHODS

The Ries crater, a 14–15 Ma (Schwarz and Lippolt 2002) complex impact crater in southeastern Germany that is 24 km in diameter (Pohl et al. 1997) (Fig. 5), has been the subject of numerous studies to characterize shocked crystalline basement rocks (e.g. Stöffler 1971; see Kring 2005 for a review). In addition, extensive impact deposits are exposed at the surface, allowing collection of a wide range of samples from crystalline megablocks and polymict breccias, to clasts in suevite. The target rocks consist of a two-layered sequence of crystalline basement rocks (mainly granites and gneisses) overlain by Mesozoic sediments. Impact deposits include low shock stage breccias (Bunte breccia), sedimentary and crystalline megablocks and monomict breccias, melt-bearing polymict breccias (fall-out and crater suevites), and localized impact melts and impact melt breccias (von Engelhardt 1990 1997; Kring 2005). Previous studies have shown that suevite deposits contain clasts of crystalline basement rocks that represent the full range of shock metamorphic stages (von Engelhardt 1990; von Engelhardt 1997). Recent work suggests that the matrix of some suevites is impact melt, which may have implications for clast annealing and re-equilibration (Osinki et al. 2004).

Samples of crystalline basement rocks (mainly granites and gneisses) were collected from outcrops of suevite, basement megablocks, and polymict crystalline breccias within and surrounding the Ries crater (the notation for these samples—for example, 080803–4.1D—includes the date of collection [8 August, 2003] and sample number [4.1D]). Additional samples from the area were also provided by Friedrich Hörz and Dieter Stöffler (Stöffler 1971; sample numbers 43–1120 in Table 2). Samples were grouped into two categories, plutonic or metamorphic, based on the presence or absence of foliation in the hand sample. However, the more detailed sample classifications used by Stöffler were retained for his sample set. Thin sections of the samples were examined optically using a petrographic microscope to characterize shock features as well as inclusions.

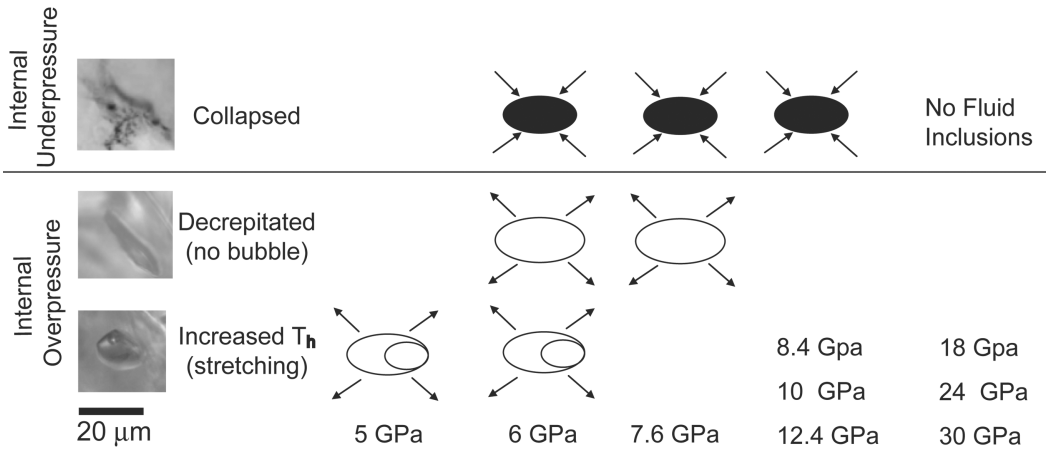

Fig. 2. Evolution of fluid inclusion features with increasing shock pressure. The bar scale shown applies to all three photomicrographs. See text for details.

Table 1. Classification of impact target rocks based on shock features, after Stöffler (1971).

Shock stage	Shock features in quartz	Pressure range (GPa)	Post-shock temperature (°C)
0	Irregular fractures	<5–10	<100
1	Planar fractures and shock lamellae	5–35	100–300
2	Diaplectic glass	35–45	300–900
3	Localized melting	45–60	900–1200
4	Whole rock melting	60–100	1200–2500
5	Vaporization	<100	>2500

Samples were classified (shock stage 1–4) based on the common presence of shock features within quartz (Table 1). Shock stage 0 samples contain no indicative shock features. Samples containing planar fractures (Figs. 6a and 6b) and/or shock lamellae or planar deformation features (Fig. 6c) were classified as shock stage 1. Planar fractures are parallel sets of fractures spaced 5–10 μm apart. Shock lamellae or planar deformation features are groups of thin (<1 μm), parallel lamellae of glass or recrystallized quartz spaced <5 μm apart. Shock stage 2 samples contain diaplectic glass (a disordered, glassy form of a mineral that preserves the original morphology of the mineral), and shock stage 3 rocks have experienced significant localized melting. Those samples constituting melt bombs that are made up nearly entirely of normal glass (a disordered, glassy form of a mineral that may involve melt flow and/or mixing with melt from adjacent minerals) were classified as shock stage 4. This classification scheme is based on that of Stöffler (1971).

Modal mineralogy (Table 2) and the frequency of quartz grains exhibiting shock features (Table 3; Fig. 7a) were quantified by point counting. Quartz grains were classified based on their maximum shock indicator. For example, a grain containing planar fractures and shock lamellae would be classified as containing shock lamellae, since these features first appear at higher shock pressures than planar fractures alone.

Quartz grains were also characterized into three categories based on the type of inclusions they contain: two-phase inclusions (liquid and vapor bubble), single-phase inclusions (mineral inclusions, melt inclusions, single-phase liquid or gas, or decrepitated inclusions), and those containing no inclusions (Table 3). These inclusion types represent an increasing level of re-equilibration, from little or no re-equilibration (two-phase fluid inclusions) to moderate re-equilibration (single-phase fluid inclusions) to high levels of re-equilibration (complete destruction of fluid inclusion vesicles). If a quartz grain contained both two-phase and single-phase inclusions, it was classified as containing two-phase inclusions; these grains were not counted a second time as containing single-phase inclusions so that the minimum level of re-equilibration within each grain was recorded. Observations and point-counting of fluid inclusions in the samples were conducted separately from point counts of modal mineralogy, shock features, and shock classification. Samples were renumbered so that the shock classification of the sample was unknown. However, in the process of examining the samples for fluid inclusions, shock features (if present) were quite apparent, making it impossible to conduct a truly "blind" study.

RESULTS

All of the shock stage 0 samples analyzed in this study contained two-phase aqueous fluid inclusions (Figs. 8b and 8c). Some two-phase inclusions appear to be associated with microcracks (MC in Fig. 8c), suggesting that they have experienced internal overpressures. However, it is unclear if these microcracks formed as a result of shock re-equilibration or were present in the target rocks prior to impact. Melt

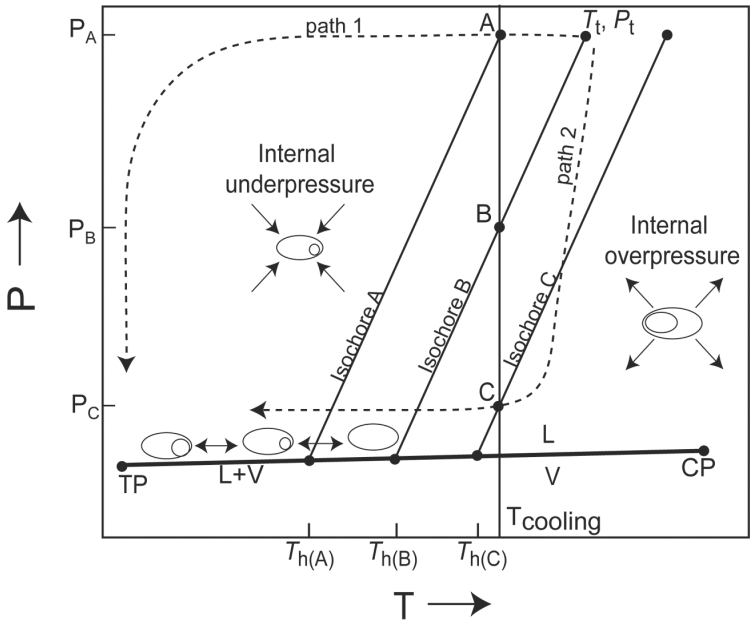

Fig. 3. Pressure-temperature conditions inside a fluid inclusion as a function of external temperature and pressure (modified after Elwood Madden et al. 2004). At any temperature (T), the pressure inside of a fluid inclusion containing both liquid and vapor is defined by the pressure along the liquid-vapor curve (line $L + V$ extending from the triple point [TP] to the critical point [CP]). Once the inclusion homogenizes, the pressure is defined by the pressure along the fluid isochore (isochore B extending from the homogenization temperature [T_{hB}] to the inclusion trapping conditions [T_t, P_t]). A fluid inclusion trapped at conditions T_t, P_t whose P-T cooling or uplift path corresponds to the fluid isochore (isochore B) will always maintain the same pressure inside of the inclusion as outside, resulting in no re-equilibration. However, if the sample follows path 1, the external pressure is always greater than the internal pressure and re-equilibration due to the internal underpressure may occur. The resulting decrease in the volume of the fluid inclusion produces an increase in fluid density (isochore A) and a decrease in homogenization temperature (T_{hA}). If the rock follows path 2, the fluid inclusion may re-equilibrate owing to internal overpressures, resulting in an increase in the size of the fluid inclusion, a decrease in fluid density (isochore C), and an increase in homogenization temperature (T_{hC}).

inclusions (Fig. 8a), mineral inclusions (likely rutile or apatite; see Fig. 8d), and single-phase inclusions (SPI in Fig. 7c) were also observed in the unshocked or weakly shocked samples. The melt inclusions observed in these rocks likely formed during crystallization of the target rocks or their protoliths and are not a result of impact melting.

Effect of Shock Stage on Fluid Inclusion Characteristics

The results of this study demonstrate that fluid inclusions in crystalline rocks may be lost due to shock re-equilibration, even at low to moderate shock pressures (shock stages 1–2). While unshocked samples from the Ries are not available due to limitations in their surface exposure, comparison of average fluid inclusion frequency between rocks of different shock stages demonstrates that fluid inclusions have been lost due to impact processing. All of the quartz grains in shock stage 0 rocks contain inclusions and nearly 70% contained two-phase fluid inclusions (Fig. 7b). However, the frequency of two-phase inclusions decreases sharply to less than 20% of quartz grains in shock stage 1 samples. The average frequency of two-phase inclusions decreases to less than one percent of quartz grains in shock stage 2 and 3 rocks (only one of six shock stage 2 rocks and two of thirteen shock stage 3 samples contained two-phase inclusions). This indicates that two-phase fluid inclusions either re-equilibrate due to non-isochoric P-T-t paths experienced during the impact event (Fig. 4) or are destroyed due to plastic deformation and phase changes within the host mineral.

While the percentage of grains containing two-phase inclusions decreases sharply between shock stage 0 and shock stage 1, the total percentage of grains containing fluid inclusions (single-phase and/or two-phase) decreases only slightly (Fig. 7b). This suggests that while some inclusions are completely destroyed, most of the two-phase inclusions have simply re-equilibrated to form single-phase inclusions, resulting in a large increase in the percentage of grains which contain only single-phase inclusions. However, between shock stage 1 and shock stage 2, the percentage of grains containing either single-phase or two-phase inclusions decreases significantly, indicating that many inclusions have been destroyed. A similar decrease is also observed in the shock stage 3 samples, where even more single-phase inclusions have been lost.

It should be noted that the frequency of both single-phase and two-phase inclusions is higher in the shock stage 4 rocks relative to shock stage 3. In these two glass bomb samples, it appears that low shocked to moderately shocked (shock stages 0–3) quartz grains have been incorporated into the melt, retaining some of their inclusions. That is, whereas the

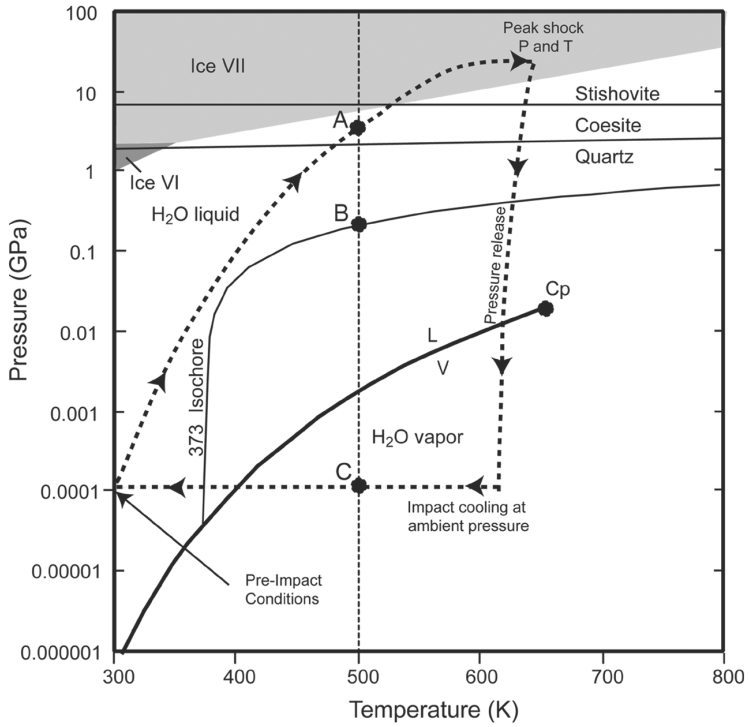

Fig. 4. Pressure-temperature-time path of quartz during a 22 GPa impact event (adapted from Elwood Madden et al. 2004). The dashed line with arrows approximates the *P-T-t* path of the sample (using data from Gratz et al. 1992). The thin line labeled "373 isochore" represents the isochore for a fluid inclusion that homogenizes at 373 K (100 °C). Stability fields for various phases of H_2O are also shown: the light gray field at high pressure shows the stability field of ice VII, and the small dark gray wedge at moderate pressure and low temperature represents the stability field of ice VI. The bold line (labeled *L*/*V*) that ends at the critical point (*Cp*) of water is the liquid-vapor curve for H_2O. Phase boundaries based on static experiments for the SiO_2 polymorphs stishovite, coesite, and quartz are shown as thin, nearly horizontal lines at elevated pressure. When the *P-T* path is above the fluid isochore (such as at point A), the fluid inclusions are underpressured, and when the *P-T* path is below the fluid isochore (such as at point C) the inclusions are overpressured (points A, B, and C are analogous to points A, B, and C in Fig. 3). Note that immediately following impact, the fluid inclusions experience a significant internal underpressure. After the high pressure shock wave has traveled through the sample and the pressure returns to ambient conditions, the temperature of the sample remains high for an extended period as the quartz slowly cools, resulting in an extended period of internal overpressure within the fluid inclusions.

rock represents shock stage 4, the clasts entrained in it may only represent shock stages 0, 1, 2, or 3. This type of heterogeneous mixing of shock metamorphosed materials is common at impact sites.

Effect of Biotite Content on Re-Equilibration Behavior

The effect of biotite content on fluid inclusion survival was also investigated. Due to its propensity to kink, the volume of individual grains of biotite can be reduced up to 20% during impact (Hörz and Ahrens 1969). This may result in biotite accommodating a disproportionate amount of the strain in a heterogeneous target, with quartz and other minerals experiencing lower levels of strain. This may also generate more waste heat in the rock and lead to higher average shock temperatures. Therefore, rocks containing high percentages of biotite may respond to shock processes differently than rocks containing no sheet silicates.

The results of this study indicate that biotite content (ranging from 0 to 35%) has little to no effect on fluid inclusion preservation (Fig. 9). Since fluid inclusion preservation is likely dependent on localized differences in shock pressure, it appears that kinking of biotite does not absorb enough strain to cushion nearby quartz grains, nor does it significantly elevate the average temperature of the rock, thus causing fluid inclusions to re-equilibrated at lower pressures. This held true for rocks in all four shock stages. However, there is a slight trend toward fewer fluid inclusions with higher biotite content in shock stage 0 samples. However, no biotite kinking was observed in these low shock pressure samples.

Effect of Grain Size on Fluid Inclusion Re-Equilibration

The effect of grain size on fluid inclusion preservation was examined. Rocks of intrinsically smaller grain size may accommodate a greater proportion of strain along grain boundaries than rocks with larger grain sizes, potentially resulting in some grain-size-dependent differences in inter- and intragranular deformation. If this is the case, fluid

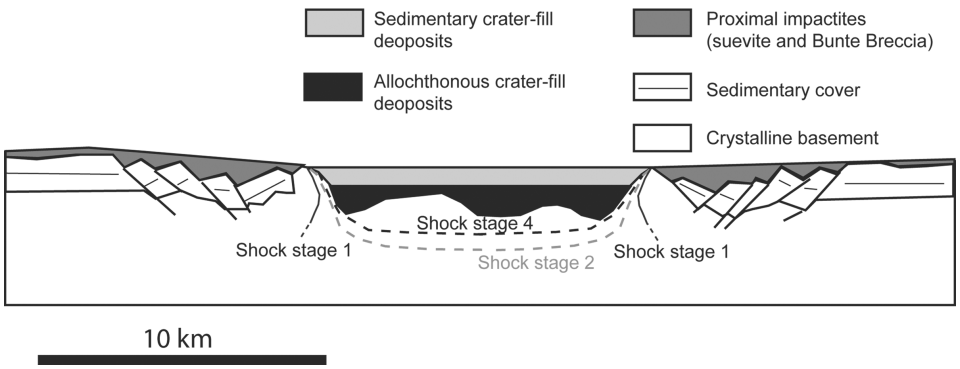

Fig. 5. Schematic cross-section of the Ries crater showing approximate shock stage isobars of interest (cross-section modified from Osinski et al. (2004), pressure estimates from Turtle and Pierazzo (1998)). Most two-phase fluid inclusions have re-equilibrated to form single-phase inclusions in shock stage 1 samples. At and above shock stage 2, most single-phase inclusions are also lost from the samples. Shock stage 4 represents whole-rock melting.

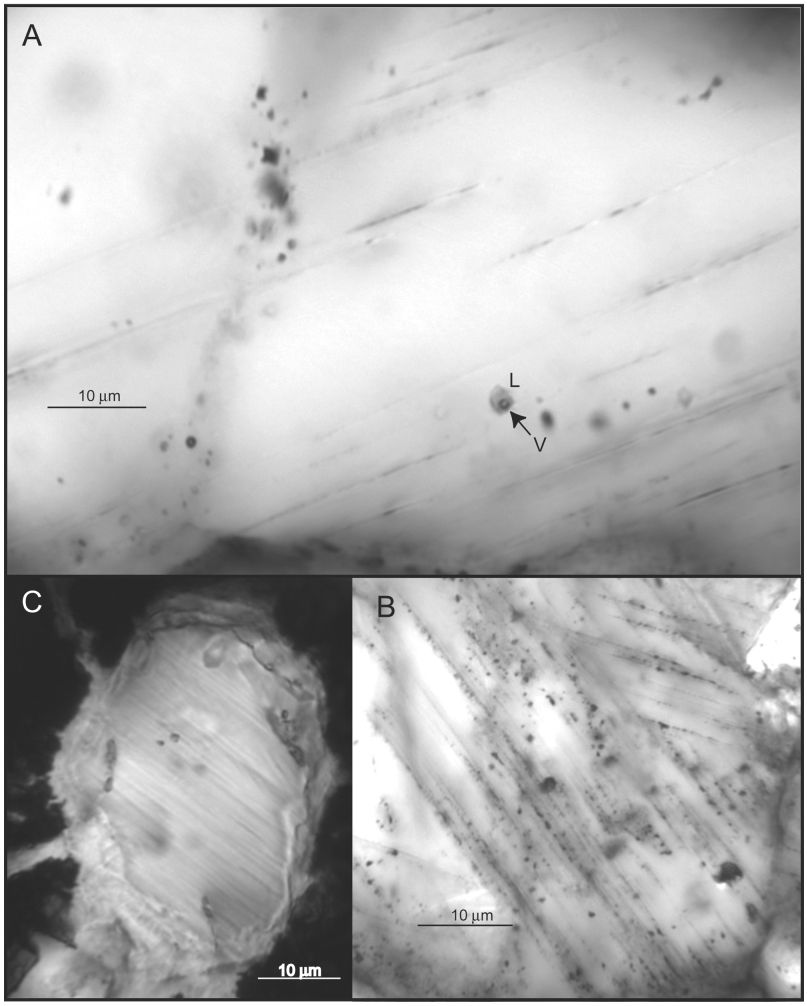

Fig. 6. Photomicrographs of shock features in quartz, illustrating the relationship of two-phase and single-phase inclusions to these features. It should be noted that most grains that contain planar fractures and/or shock lamellae do not contain inclusions and that the cases illustrated are somewhat atypical. a) Two-phase fluid inclusions are observed in a few grains which also contain planar fractures (shock stage 1, sample RIE090803–1.1 from polymict breccia at Myers Keller near Noerdlinglen). Single-phase inclusions are also observed in grains with (b) decorated planar fractures (shock stage 1, sample 316 collected by Stöffler from Zipplingen) and (c) shock lamellae (shock stage 3, sample RIE080803–1.1I from Amuehle).

Table 2. Location and mineralogy of crystalline basement target rocks examined in this study.

Sample number	Location	Sample context[a]	Sample lithology[b]	Shock stage	Grain size (mm)	Quartz	Biotite	Feldspar	Mafics	Garnet	Calcite	Opaque
080803–4.1D	Wenneburg	Monomict breccia	Granite	0	0.27	36.5	13.5	50	0	0	0	0
030803–1.1	Lehburg	Basement megablock	Granite	0	0.36	50.9	1.9	47.2	0	0	0	0
080803–4.1B	Wenneburg	Monomict breccia	Granite	0	0.22	38.9	18.5	40.7	1.9	0	0	0
689	Langenmuehle		Biotite granite	0	0.34	37.5	20	42.5	0	0	0	0
719	Wegenhausen		Biotite granite	0	0.15	41.3	2.5	51.3	5	0	0	0
43	Aumuehle	Suevite	Leuco granite	0	0.2	38.6	3.5	57.9	0	0	0	0
600	Otting	Suevite	Biotite monzodiorite	0	0.24	28.9	17.8	46.7	4.4	0	2.2	0
136	Schratten Hofen		Leuco granite	0	0.4	44.2	1.9	53.8	0	0	0	0
1120	Albuck		Amphibolite	0	0.18	10.9	0	43.6	43.6	0	1.8	0
725	Minderoffingen		Granite	0	0.35	35.8	9	55.2	0	0	0	0
851	Huernheim		Hornblende gneiss	0	0.2	38.9	0	50	11.1	0	0	0
030803–1.2	Lehburg	Basement megablock	Gneiss	0	0.46	54.8	26.2	7.1	0	11.9	0	0
030803–1.7	Lehburg	Suevite	Gneiss	0	0.25	45.3	32.8	17.2	0	4.7	0	0
090803–1.1	Meyers Keller	Polymict breccia	Granite	1	0.18	50.9	25.5	23.6	0	0	0	0
080803–1.1F	Amuehle	Suevite	Granite	1	0.32	71.2	9.6	19.2	0	0	0	0
030803–1.6	Lehburg	Basement megablock[c]	Granite	1	0.31	52.9	2.9	44.1	0	0	0	0
604	Otting	Suevite	Leuco granite	1	0.27	46	4	50	0	0	0	0
633	Alerheim		Leuco granite	1	0.35	54.9	3.9	41.2	0	0	0	0
316	Zipplingen	Suevite	Hornblende gneiss	1	0.28	55.2	6.9	37.9	0	0	0	0
030803–4.1C	Meyers Keller	Polymict breccia	Gneiss	1	0.35	68.1	12.8	19.1	0	0	0	0
397	Zipplingen	Suevite	Gneiss	1	0.25	65.8	0	34.2	0	0	0	0
44	Alteburg		Granite	2	0.34	39.5	15.8	39.5	0	0	0	0
080803–1.1E	Amuehle	Suevite	Granite	2	0.25	47.7	13.6	36.4	0	0	0	0
030803–4.1B	Meyers Keller	Polymict breccia	Granite	2	0.2	36.7	24.5	22.4	10.2	0	0	0
030803–4.1D	Meyers Keller	Polymict breccia	Granite	2	0.19	52.7	25.7	13.5	8.1	0	0	0
030803–2.1E	Amuehle	Suevite	Gneiss	2	0.22	47.6	11.9	40.5	0	0	0	0
040803–2.3B	Aufhausen	Suevite	Gneiss	2	0.08	35.4	12.5	27.1	2.1	0	0	20.8
742	Aumuehle	Suevite	Biotite gneiss	2	0.09	40.3	35.5	24.2	0	0	0	0
156	Aumuehle	Suevite	Granite	3	0.27	34	12.8	12.8	0	0	0	0
040804–2.3K	Aufhausen	Suevite	Granite	3	0.06	27.6	0	0	0	0	10.3	0
040803–2.3L	Aufhausen	Suevite	Granite	3	0.46	36.9	3.1	0	0	0	18.5	0
080803–1.1H	Amuehle	Suevite	Granite	3		20	31.1	4.4	2.2	0	0	0
080803–1.1I	Amuehle	Suevite	Gneiss	3	0.1	48.9	6.7	24.4	0	0	0	0

Table 2. *Continued.* Location and mineralogy of crystalline basement target rocks examined in this study.

Sample number	Location	Sample context[a]	Sample lithology[b]	Shock stage	Grain size (mm)	Quartz	Biotite	Feldspar	Mafics	Garnet	Calcite	Opaque
080803–1.1G	Amuehle	Suevite	Gneiss	3	0.37	40	0	31.1	0	0	0	0
040803–2.3H	Aufhausen	Suevite	Gneiss	3	0.11	6.1	34.7	26.5	0	0	2	0
090803–3.1A	Seelbronn	Suevite	Gneiss	3	0.13	33.3	6.3	8.3	0	0	0	0
080803–1.1A	Amuehle	Suevite	Gneiss	3	0.09	4.9	31.1	19.7	0	1.6	0	1.6
090803–3.1	Seelbronn	Suevite	Gneiss	3	0.3	3.8	9.6	51.9	26.9	0	7.7	0
658	Otting	Suevite	Gneiss	3	0.2	26.1	19.6	0	8.7	0	2.2	0
603	Otting	Suevite	Hornblende gneiss	3	0.23	22.4	10.2	8.2	0	0	8.2	0
149	Otting	Suevite	Hornblende gneiss	3	0.18	20.5	9.1	13.6	27.3	0	0	11.4
618	Otting	Suevite	Glass bomb	4		33.3	0	2.4	0	0	0	0
620	Otting	Suevite	Glass bomb	4		36.6	0	2.4	0	0	0	0

[a]Impact lithology of the outcrop where sample was collected. Description of impact lithology for samples collected by D. Stöffler taken from Stöffler and Ostertag (1983) where available.
[b]Rock type determined by the presence or absence of foliation for most samples, however, more detailed sample classifications were retained from Stöffler (1971) where applicable.
[c]Sample taken from along a fault plane within the outcrop.

Table 3. Percent of quartz grains containing shock features and inclusions.

			Shock features						Inclusions		
Sample no.	Shock stage	Grain size (mm)	No shock	Irregular fractures	Planar fractures	Shock lamellae	Diaplectic glass	Normal glass	Two-phase	Single-phase	No inclusions
080803–4.1D	0	0.27	10.5	89.5	0	0	0	0	55	45	0
030803–1.1	0	0.36	63	37	0	0	0	0	75.9	24.1	0
080803–4.1B	0	0.22	42.9	57.1	0	0	0	0	66.7	33.3	0
689	0	0.34	13.3	86.7	0	0	0	0	81.3	18.8	0
719	0	0.15	42.4	57.6	0	0	0	0	78.8	21.2	0
43	0	0.2	0	100	0	0	0	0	72.7	27.3	0
600	0	0.24	0	100	0	0	0	0	53.8	46.2	0
136	0	0.4	56.5	43.5	0	0	0	0	87.5	12.5	0
1120	0	0.18	0	100	0	0	0	0	16.7	83.3	0
725	0	0.35	54.2	45.8	0	0	0	0	92	8	0
851	0	0.2	66.7	33.3	0	0	0	0	100	0	0
030803–1.2	0	0.46	52.2	47.8	0	0	0	0	54.5	45.5	0
030803–1.7	0	0.25	55.2	44.8	0	0	0	0	62.1	37.9	0
090803–1.1	1	0.18	0	21.4	67.9	10.7	0	0	44.4	55.6	0
080803–1.1F	1	0.32	0	21.6	45.9	32.4	0	0	0	88.9	11.1
030803–1.6	1	0.31	5.6	61.1	33.3	0	0	0	44.4	55.6	0
604	1	0.27	0	8.7	43.5	47.8	0	0	9.1	86.4	4.5
633	1	0.35	0	75	17.9	7.1	0	0	18.5	77.8	3.7
316	1	0.28	6.3	25	43.8	25	0	0	12.5	75	12.5
030803–4.1C	1	0.35	3.1	6.3	37.5	50	3.1	0	6.3	71.9	21.9
397	1	0.25	48	12	12	28	0	0	0	53.8	46.2
44	2	0.34	0	0	0	20	80	5.3	0	26.7	73.3
080803–1.1E	2	0.25	0	0	9.5	61.9	28.6	2.3	0	15	85
030803–4.1B	2	0.2	0	0	27.8	44.4	27.8	6.1	0	38.9	61.1

Table 3. *Continued.* Percent of quartz grains containing shock features and inclusions.

			Shock features						Inclusions		
Sample no.	Shock stage	Grain size (mm)	No shock	Irregular fractures	Planar fractures	Shock lamellae	Diaplectic glass	Normal glass	Two-phase	Single-phase	No inclusions
030803–4.1D	2	0.19	2.6	2.6	20.5	61.5	12.8	0	0	61.8	38.2
030803–2.1E	2	0.22	0	0	10	50	40	0	0	30	70
040803–2.3B	2	0.08	0	5.9	5.9	35.3	52.9	2.1	5.6	44.4	50
742	2	0.09	0	0	0	84	16	0	0	4	96
156	3	0.27	0	0	0	0	100	40.4	0	0	100
040804–2.3K	3	0.06	0	0	0	0	100	62.1	0	0	100
040803–2.3L	3	0.46	0	0	0	12.5	87.5	41.5	0	8.3	91.7
080803–1.1H	3		0	0	0	11.1	88.9	42.2	0	0	100
080803–1.1I	3	0.1	9.1	0	18.2	18.2	54.5	20	4.5	31.8	63.6
080803–1.1G	3	0.37	0	0	0	5.6	94.4	28.9	0	5.6	94.4
040803–2.3H	3	0.11	0	0	33.3	33.3	33.3	30.6	0	0	100
090803–3.1A	3	0.13	18.8	18.8	6.3	0	56.3	52.1	5.9	35.3	58.8
080803–1.1A	3	0.09	0	0	33.3	0	66.7	41	0	0	100
090803–3.1	3	0.3	0	0	0	0	100	0	0	0	100
658	3	0.2	0	0	8.3	0	91.7	43.5	0	0	100
603	3	0.23	0	0	0	0	100	51	0	0	100
149	3	0.18	0	11.1	33.3	11.1	44.4	18.2	0	11.1	88.9
	4		2.4	17.1	2.4	12.2	65.9	0	7.3	9.8	82.9
620	4		2.6	25.6	2.6	7.7	61.5	2.4	0	21.6	78.4

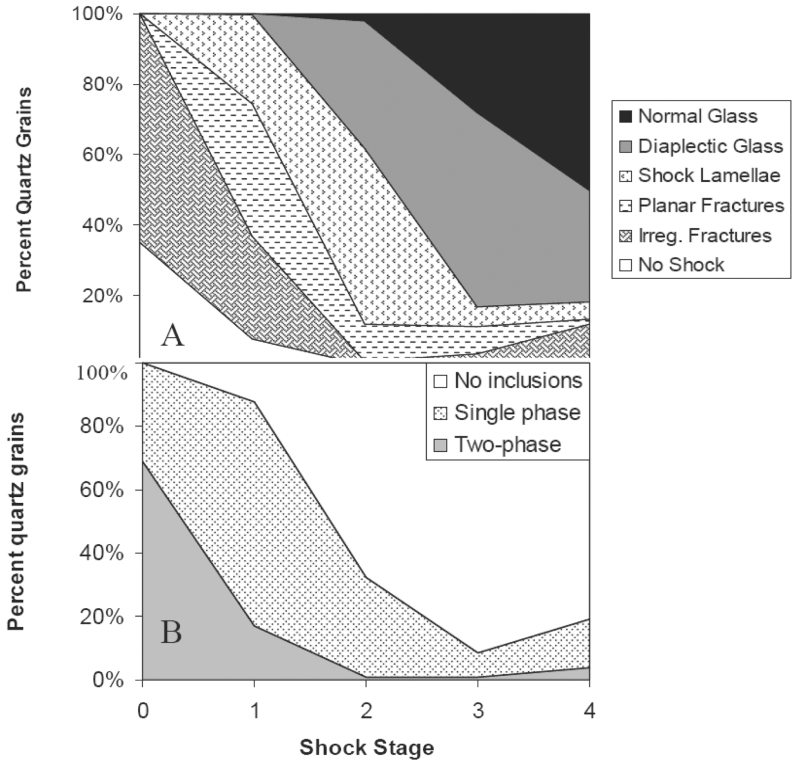

Fig. 7. a) Shock features observed in quartz grains with increasing shock stage. The relative proportions of grains containing planar fractures and shock lamellae are based on flat stage thin section observations which represent minimum values. b) The frequency of quartz grains containing inclusions with increasing shock stage. The frequency of two-phase fluid inclusions decreases sharply from shock stage 0 to shock stage 1 while single-phase inclusions increase and the total fluid inclusion count decreases only slightly. This suggestes that two-phase inclusions are reequilibrating to form single-phase inclusions due to shock metamorphism. At higher shock pressure, the frequency of single-phase inclusions also decreases sharply, indicating that fluid inclusion vesicles are destroyed due to plastic deformation and phase changes within the host minerals. The presence of two-phase inclusions within entrained quartz grains in melt clasts demonstrates the hetrogenous nature of shock deformation within the target rocks and the rapid quenching of the Ries melts.

inclusions may be more likely to be preserved in host rocks with smaller average grain sizes, as intergranular deformation may dominate.

Analysis of fluid inclusion preservation as a function of grain size within this sample set shows no evidence that grain size affects fluid inclusion reequlibration or preservation (Fig. 10). In crystalline basement rocks, deformation along grain boundaries may not be as important as in porous sediments due to the interlocking nature of the grain boundaries.

DISCUSSION

Comparison with Single Crystal Shock Experiments

Single-crystal and polycrystalline shock experiments are routinely used to calibrate the pressure and temperature conditions at which indicative shock features are likely to form. However, shock experiments are limited by the time scale over which target rocks are compressed and unloaded. The results of this study indicate that fluid inclusions in naturally impacted crystalline basement rocks re-equilibrate in a manner similar to that observed in previous single crystal shock experiments (Elwood Madden et al. 2004). Below the HEL, fluid inclusions re-equilibrate due to extreme internal overpressures or underpressures resulting from non-isochoric pressure-temperature conditions and fluid is lost along fractures in the host mineral. Above the HEL, inclusion cavities are destroyed due to deformation and phase changes within the host mineral. This may be a result of the destruction of the crystal lattice with increasing shock pressure (Hörz and Quaide 1973)

In single crystal experiments, two-phase inclusions were not observed in samples shocked to greater than 6 GPa and all evidence of previous fluid inclusions was lost in samples shocked above 12 GPa. In the naturally shock-metamorphosed crystalline rocks examined in this study, some two-phase inclusions are observed in shock stage 1 rocks (10–35 GPa). However, most have re-equilibrated to form single-phase inclusions, leading to an increase in the frequency of single-phase inclusions, but only a small net loss of inclusions from these samples. In addition, single-phase inclusions were frequently observed in samples of shock stages 2 and 3 crystalline basement rocks, suggesting that

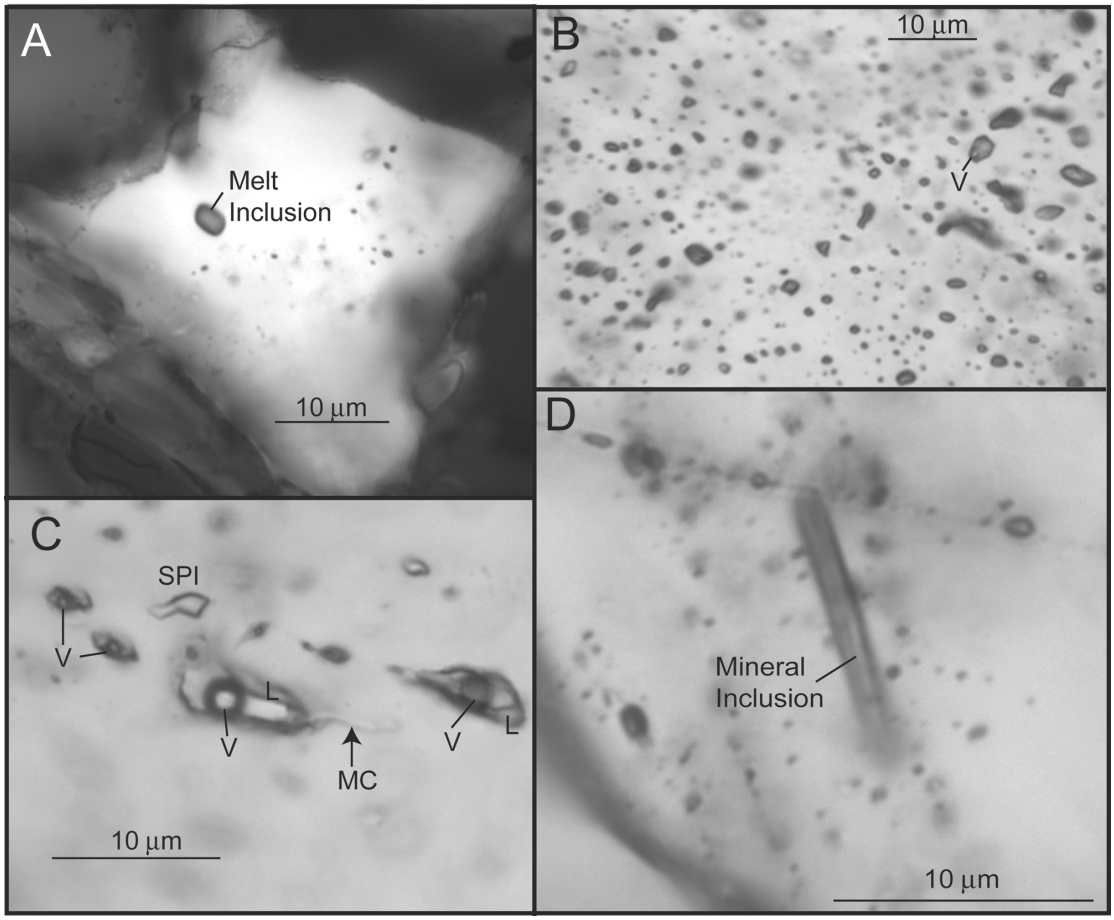

Fig. 8. Photomicrographs of inclusions in quartz. a) Melt inclusions (sample RIE030803–1.2 collected from Lehburg), single-phase aqueous inclusions (SPI in [c] sample 136 collected by Stöffler from Schratten Hofen), b) and c) two-phase aqueous inclusions (in [b]: sample 698 collected by Stöffler from Langenmuehle), and d) mineral inclusions of rutile and apatite (sample RIE030803–1.1 collected from Lehburg) were observed in shock stage 0 rocks. Two-phase inclusions contain a liquid phase (*L*) and a vapor bubble (*V*), while melt inclusions, mineral inclusions, and single-phase inclusions do not contain a vapor bubble.

single-phase inclusions within quartz grains that experience little or no deformation may be preserved even though the average shock pressure for the host rock likely exceeded 20 GPa. This wide range of shock effects within polycrystalline samples has been observed in several other studies that compared natural impactites with single-crystal shock experiments; this is likely a result of local heterogeneities in shock pressure distribution caused by impedance contrasts between neighboring grains and reflections through the rock (Grieve et al. 1996; Stöffler 1971).

Comparison with Porous Sedimentary Target Rocks

The authors of this study are also currently investigating the effects of shock metamorphism on fluid inclusions trapped in porous sedimentary target rocks. Samples of Coconino sandstone were collected from the Barringer crater (Meteor Crater), Arizona, and analyzed following similar methods described above (Elwood Madden et al. 2006). The results from the study of sedimentary rocks are similar to those observed in this work on crystalline basement lithologies. Two-phase fluid inclusions are extremely rare in samples of Coconino sandstone that contain planar fractures. No two-phase inclusions were observed in samples containing shock lamellae and/or diaplectic glass. In addition, the frequency of single-phase fluid inclusions decreases dramatically in samples containing diaplectic glass. The effects of shock re-equilibration on fluid inclusions in sedimentary rocks appear to be more homogeneous than for crystalline targets; however, some degree of variability is still observed. Comparison of the two data sets also suggests that destruction of fluid inclusions in sedimentary rocks begins at slightly lower shock pressures, since single-phase inclusions were observed in crystalline basement rocks which contained shock lamellae. However, it is difficult to directly compare the two sample sets, since shock lamellae are not as common in sedimentary rocks and may require higher shock pressures in order to form (French 1998; Grieve et al. 1996; Kieffer 1971).

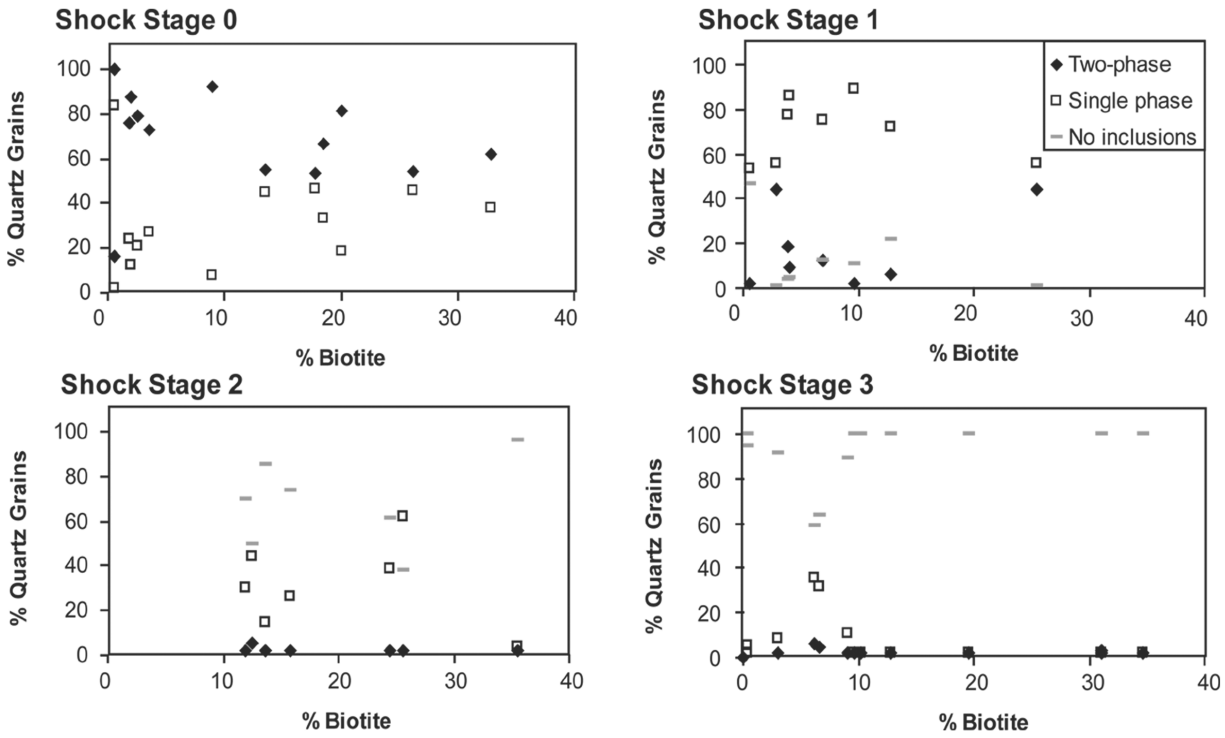

Fig. 9. Fluid inclusion frequency versus biotite content of rocks within shock stages 0–3. In the shock stage 0 samples, the frequency of quartz grains containing two-phase inclusions decreases slightly as biotite content increases. However, biotite content appears to have no effect on fluid inclusion preservation in shock stages 1–3.

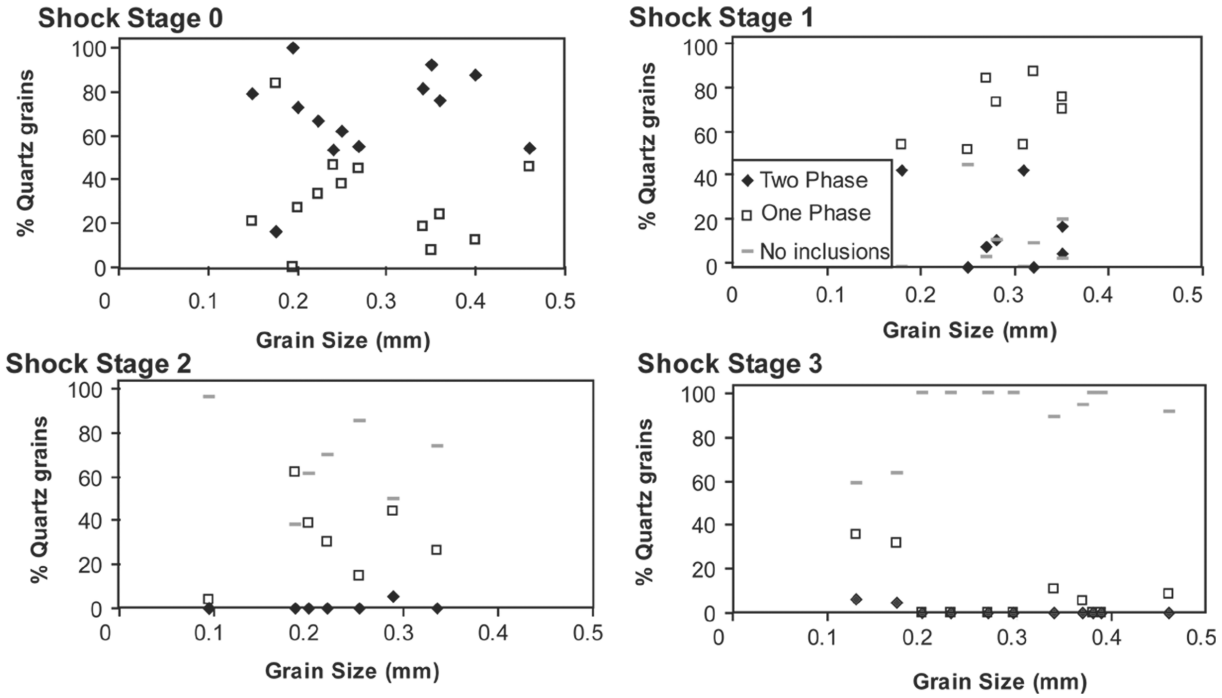

Fig. 10. Fluid inclusion frequency versus grain size within shock stages 0–3. Within shock stages 0–2, grain size appears to have no effect on the preservation of fluid inclusions in quartz. There is some evidence in shock stage 3 rocks that fluid inclusions may be more likely to survive in rocks with a smaller grain size.

Shock Devolatilization

The re-equilibration and destruction of fluid inclusions that occurs during shock metamorphism results in the loss of fluid contained within impacted materials and may also result in the redistribution of fluids or shock devolatilization of crystalline target rocks. Terrestrial rocks often contain on the order of .001–1 vol% fluid inclusion vesicles (Roedder 1984). Therefore, a 1 km^3 volume of rock may contain up to 10^7 m^3 of water trapped in fluid inclusions. As these fluid inclusions re-equilibrate, the fluid contained within the inclusions may be lost from the host rock along fractures and microcracks. Therefore, even in shock stage 0 and shock stage 1 rocks (<10 GPa; see Fig. 5), a significant amount of fluid may be lost from fluid inclusions. In addition, the destruction of fluid inclusion vesicles due to plastic deformation and possibly phase changes in the host mineral at higher pressures (>30 GPa, see Fig. 5) may lead to additional water loss. As a result, shock re-equilibration and destruction of fluid inclusions in crystalline target rocks likely contributed to the devolatilization of early planetismals and redistribution of water in terrestrial rocks during the period of heavy bombardment.

Parnell et al. (2005) recently described hydrocarbon-bearing fluid inclusions in dolomite-rich host rocks from the Haughton impact structure. The authors assumed that the fluid inclusions were trapped prior to impact because similar fluid inclusions occur in the surrounding rocks, even though the impacted rocks experienced shock pressures exceeding 10 GPa. However, the results of this study of crystalline basement target rocks, combined with previous experimental work and a concurrent study of porous sedimentary target rocks (Elwood Madden et al. 2006), suggest that fluid inclusions begin to re-equilibrate at low shock pressures and that most fluid inclusions are destroyed at shock pressure greater than 10–12 GPa. Therefore, it is unlikely that the fluid inclusions described by Parnell et al. (2005) represent pristine, pre-impact fluid inclusions. Recent studies of fluid inclusions and alteration phases in hydrothermal veins in the Chicxulub impact crater demonstrate that post-impact hydrothermal activity can redistribute fluids and alter rocks within an impact crater (Lueders and Rickers 2004; Zuercher and Kring 2004). In the case of the Haughton impact structure, post-impact hydrothermal activity may have led to regional migration of hydrocarbons through rocks within the impact crater as well as the surrounding area. If this is the case, the temperatures recorded by the biomarkers do not constrain the maximum temperature associated with the impact event, but they might represent maximum temperatures associated with subsequent hydrothermal activity.

Fluid Inclusions in Other Minerals

This study, along with the previous experimental work, has focused on shock re-equilibration of fluid inclusions trapped in quartz. While quartz is abundant in the Earth's crust and is commonly found in terrestrial impactites, it is seldom found in meteorites and planetary materials. However, the results of these studies can be used to evaluate the re-equilibration behavior of fluid inclusions trapped in host minerals other than quartz that may be more common target minerals in meteorites and other planets.

The magnitude of the pressure differential (external load on the host mineral compared to the fluid pressure within inclusions) required to re-equilibrate fluid inclusions is dependent on the bulk modulus and cleavage properties of the host mineral as well as the size and shape of the inclusion and the absolute distance of the inclusions from free surfaces (Bodnar et al. 1989; Tugarinov and Naumov 1970; Ulrich and Bodnar 1988; Zhang 1998; Bodnar 2003; Burnley and Davis 2004). Therefore, fluid inclusions trapped in olivine are likely to survive greater pressure gradients than those trapped in quartz, since olivine has a higher bulk modulus and similar lack of cleavage. However, fluid inclusions trapped in calcite or other carbonates are likely to begin to re-equilibrate at lower pressure gradients due to cleavage and deformation of the host mineral.

The pressure at which elastic deformation ceases and plastic deformation begins (the HEL) appears to be the most important factor in determining whether or not single-phase inclusions will be preserved in impacted rocks (Elwood Madden et al. 2004). Therefore, fluid inclusions may be preserved at higher shock pressures in minerals with an HEL greater than quartz. Alternatively, in minerals such as carbonates with HEL's less than quartz, fluid inclusions may be destroyed by plastic deformation at much lower shock pressures.

CONCLUSIONS

The results of this study demonstrate that two-phase fluid inclusions in crystalline basement rocks re-equilibrated to form single-phase inclusions at low to moderate shock pressures (shock stages 1–2). As shock pressure increases, host minerals undergo plastic deformation and phase changes, destroying inclusion vesicles and leaving no evidence of fluid inclusions that may have been present prior to impact. Therefore, the relative scarcity of fluid inclusions in planetary materials may be a result of impact processing and may not reflect the absence of water on the parent body. Re-equilibration and eventual destruction of fluid inclusions with increasing shock pressures may have contributed significantly to shock devolatilization of early planetismals and liberated water from terrestrial impactites.

Biotite (or sheet silicate) abundance from 0–35% appears to have no effect on fluid inclusion preservation, except in shock stage 0 samples where two-phase inclusion frequency decreased slightly as biotite content increased. Target rock grain size also had little to no effect on fluid inclusion preservation.

Fluid inclusions in naturally shock metamorphosed crystalline basement rocks follow a progression of re-equilibration to produce single-phase inclusions at low shock pressures (shock stage 1), to complete destruction of inclusion vesicles in moderately to highly shocked rocks (shock stages 2–4), similar to that observed in experimental studies. However, the inclusions in this study survive slightly higher shock pressures than those in experimentally shocked single-crystal quartz. Shock re-equilibration behavior of fluid inclusions in crystalline basement rocks observed in this study is similar to that observed for fluid inclusions in porous sedimentary target rocks.

Acknowledgments–We would like to thank D. Stöffler and F. Hörz for providing some of the samples used in this study and their shock classification. We would also like to thank F. Hörz for his helpful advice throughout the course of this study. Suggestions from associate editor John Spray as well as comments from reviewers M. Zolensky and D. Vanka strengthened the manuscript. MEEM received support from the Barringer Family Fund for Meteorite Impact Research and a student travel grant from the Meteoritical Society for field work. MEEM was also partially supported by a Virginia Tech ADVANCE fellowship. A modest level of support was provided by NASA grant NAG5–12881 to D. A. K. and NSF grants EAR–0125918 and EAR–0337094 to R. J. B.

Editorial Handling—Dr. John Spray

REFERENCES

Andersen T. and Burke E. A. J. 1996. Methane inclusions in shocked quartz from the Gardnos impact breccia, South Norway. *European Journal of Mineralogy* 8:927–936.

Bibring J.-P., Langevin Y., Gendrin A., Gondet B., Poulet F., Berthe M., Soufflot A., Arvidson R., Mangold N., Mustard J., and Drossart P. 2005. Mars surface diversity as revealed by the OMEGA/Mars Express observations. *Science* 307:1576–1581.

Bodnar R. J. 1999. Fluid inclusions in ALH 84001 and other Martian meteorites: Evidence for volatiles on Mars (abstract #1222). 30th Lunar and Planetary Science Conference. CD-ROM.

Bodnar R. J. 2003. Reequilibration of fluid inclusions. In *Fluid inclusions: Analysis and interpretation*. Ottawa: Mineralogical Association of Canada. pp. 213–231.

Bodnar R. J., Binns P. R., and Hall D. L. 1989. Synthetic fluid inclusions. VI. Quantitative evaluation of the decrepitation behavior of fluid inclusions in quartz at one atmosphere confining pressure. *Journal of Metamorphic Geology* 7:229–242.

Bridges J. C., Catling D. C., Saxton J. M., Swindle T. D., Lyon I. C., and Grady M. M. 2001. Alteration assemblages in Martian meteorites: Implications for near-surface processes. *Space Science Reviews* 96:365–392.

Burnley P. C. and Davis M. K 2004. Volume changes in fluid inclusions produced by heating and pressurization: An assessment by finite element modeling. *Canadian Mineralogist* 42:1369–1382.

Carr M. H., Belton M. J., Chapman C. R., Davies M. E., Geissler P., Greenberg R., McEwen A. S., Tufts B. R., Greeley R., Sullivan R., Head J. W., Pappalardo R. T., Klaasen K. P., Senske T. V., Kaufman J., Senske D., Moore J., Neukum G., Schubert G., Burns J. A., Thomas P., and Veverka J. 1998. Evidence for a subsurface ocean on Europa. *Nature* 391: 363–365.

Elwood Madden M. E., Kring D. A., and Bodnar R. J. 2006. Shock reequilibration of fluid inclusions in Coconino Sandstone from Meteor Crater, Arizona. *Earth and Planetary Science Letters* 241:32–46.

Elwood Madden M. E., Hörz F., and Bodnar R. J. 2004. Experimental simulation of shock-induced re-equilibration of fluid inclusions. *Canadian Mineralogist* 42:1357–1368.

Endress M., Zinner E., and Bischoff A. 1996. Early aqueous activity on primitive meteorite parent bodies. *Nature* 379:701–703.

Feldman W. C., Boynton W. V., Tokar R. L., Prettyman T. H., Gasnault O., Squyres S. S. W., Elphic R. C., Lawrence D. J., Lawson S. L., Maurice S., McKinney G. W., Moore K. R., and Reedy R. C. 2002. Global distribution of neutrons from Mars: Results from Mars odyssey. *Science* 297:75–78.

Fredriksson K. and Kerridge J. F. 1988. Carbonates and sulfates in CI chondrites: Formation by aqueous activity on the parent body. *Meteoritics* 23:35–44.

French B. M. 1998. *Traces of catastrophe: A handbook of shock metamorphic effects in terrestrial meteorite impact structures*. Houston: Lunar and Planetary Institute. 120 p.

Golombek M. P., Cook R. A., Economou T., Folkner W. M., Haldemann A. F. C., Kallemeyn P. H., Knudsen J. M., Manning R. M., Moore H. J., Parker T. J., Rieder R., Schofield J. T., Smith P. H., and Vaughan R. M. 1997. Overview of the Mars Pathfinder Mission and assessment of landing site predictions. *Science* 278: 1743–1748.

Gratz A. J., Nellis W. J., Christie J. M., Brocious W., Swegle J., and Cordier P. 1992. Shock metamorphism of quartz with initial temperatures −170 to +1000 Deg C. *Physics and Chemistry of Minerals* 19:267–88.

Grieve R. A. F., Langenhorst F., and Stöffler D. 1996. Shock metamorphism of quartz in nature and experiment: II. Significance in geoscience. *Meteoritics & Planetary Science* 31: 6–35.

Hode T., von Dalwigk I., and Broman C. 2003. A hydrothermal system associated with the Siljan impact structure, Sweden-implications for the search for fossil life on Mars. *Astrobiology* 3:271–289.

Hörz F. and Ahrens T. J. 1969. Deformation of experimentally shocked biotite. *American Journal of Science* 267:1213–1229.

Hörz F. and Quaide W. L. 1973. Debze-Scherrer investigation of experimentally shocked silicates. *The Moon* 6:45–82.

Keller L. P., Thomas K. L., Clayton R. N., Mayeda T. K., DeHart J. M. and McKay D. S. 1984. Aqueous alteration of the Bali CV3 chondrite: Evidence from mineralogy, mineral chemistry, and oxygen isotopic compositions. *Geochimica et Cosmochimica Acta* 58:5589–98.

Kieffer S. W. 1971. Shock metamorphism of the Coconino sandstone at Meteor Crater, Arizona. *Journal of Geophysical Research* 76: 5449–5473.

Kirsimae K., Suuroja S., Kirs J., Karki A., Polikarpus M., Puura V., and Suuroja K. 2002. Hornblende alteration and fluid inclusions in Kärdla impact crater, Estonia: Evidence for impact-induced hydrothermal activity. *Meteoritics & Planetary Science* 37:449–457.

Koeberl C., Fredriksson K., Goetzinger M., and Reimold W. U. 1989. Anomalous quartz from the Roter Kamm impact crater, Namibia: Evidence for post-impact hydrothermal activity? *Geochimica et Cosmochimica Acta* 53:2113–2118.

Komor S. C., Valley J. W., and Brown P. E. 1988. Fluid-inclusion evidence for impact heating at the Siljan Ring, Sweden. *Geology* 16:711–715.

Kring D. A. 2005. Hypervelocity collisions into continental crust composed of sediments and underlying crystalline basement: Comparing the Ries (~24 km) and Chicxulub (~180 km) impact craters. *Chemie der Erde* 65:1–46.

Langenhorst F. 1994. Shock experiments on pre-heated a- and b-quartz: II. X-ray and TEM investigations. *Earth and Planetary Science Letters* 128:683–98.

Lueders V. and Rickers K. 2004. Fluid inclusion evidence for impact-related hydrothermal fluid and hydrocarbon migration in Cretaceous sediments of the ICDP-Chicxulub drill core Yax-1. *Meteoritics & Planetary Science* 39:1187–1197.

Malin M. C., Carr M. H., Danielson G. E., Davies M. E., Hartmann W. K., Ingersoll A. P., James P. B., Masursky H., McEwen A. S., Soderblom L. A., Thomas P., Veverka J., Caplinger M. A., Ravine M. A., Soulanille T. A., and Warren J. L. 1998. Early views of the martian surface from the Mars Orbiter Camera of Mars Global Surveyor. *Science* 279:1681–1685.

Osinski G. R., Grieve R. A. F., and Spray J. G. 2004. The nature of the groundmass of surficial suevite from the Ries impact structure, Germany, and constraints on its origin. *Meteoritics & Planetary Science* 39:1655–1683.

Parnell J., Osinski G. R., Lee P., Green P. F., and Baron M. J. 2005. Thermal alteration of organic matter in an impact crater and the duration of postimpact heating. *Geology* 33:373–376.

Pohl J., Stöffler D., Gall H., and Ernston K. 1977. The Ries impact crater. In *Impact and explosion cratering*, edited by Merrill R. B. New York: Pergamon Press. pp. 343–404.

Porco C. C., Baker E., Barbara J., Beurle K., Brahic A., Burns J. A., Charnoz S., Cooper N., Dawson D. D., Del Genio A. D., Denk T., Dones L., Dyudina U., Evans M. W., Fussner S., Giese B., Grazier K., Helfenstein P., Ingersoll A. P., Jacbson R. A., Johnston T. V., McEwen A., Murray C. D., Neukum G., Owen W. M., Perry J., Roatsch T., Spitale J., Squyres S., Thomas P., Tiscareno M., Turtle E. P., Vasavada A. R., Veverka J., Wagner R., and West R. 2005. Imaging of Titan from the Cassini spacecraft. *Nature* 434:159–168.

Roedder E. 1984. *Fluid inclusions*. Chantilly, Virginia: Mineralogical Society of America. 644 p.

Rubin A. E., Zolensky M. E., and Bodnar R. J. 2002. The halite-bearing Zag and Monahans (1998) meteorite breccias: Shock metamorphism, thermal metamorphism and aqueous alteration on the H-chondrite parent body. *Meteoritics & Planetary Scienc*e 37:125–141.

Schwartz W. H. and Lippolt H. J. 2002. Coeval argon-40/argon-39 ages of moldavites from the Bohemian and Lusatian strewn fields. *Meteoritics & Planetary Science* 37:1757–1763.

Soffen G. A. 1976. Scientific results of the Viking missions. *Science* 194:1274–1276.

Squyres S. W., Arvidson R. E., Bell J. F. III, Bruckner J., Cabrol N. A., Calvin W., Carr M. H., Christensen P. R., Clark B. C., Crumpler L., Marais D. J. D., d'Uston C., Economou T., Farmer J., Farrand W., Folkner W., Golombek M., Gorevan S., Grant J. A., Greeley R., Grotzinger J., Haskin L., Herkenhoff K. E., Hviid S., Johnson J., Klingelhofer G., Knoll A. H., Landis G., Lemmon M., Li R., Madsen M. B., Malin M. C., McLennan S. M., McSween H. Y., Ming D. W., Moersch J., Morris R. V., Parker T., Rice J. W., Jr., Richter L., Rieder R., Sims M., Smith M., Smith P., Soderblom L. A., Sullivan R., Wanke H., Wdowiak T., Wolff M., and Yen A. 2004. The Opportunity Rover's Athena science investigation at Meridiani Planum, Mars. *Science* 306:1698–1703.

Stöffler D. 1971. Progressive metamorphism and classification of shocked and brecciated crystalline rocks in impact craters. *Journal of Geophysical Research* 76:5541–5551.

Stöffler D., Artemieva N. A., and Pierazzo E. 2002. Modeling the Ries-Steinheim impact event and the formation of the moldavite strewn field. *Meteoritics & Planetary Science* 37:1893–1907.

Stöffler D. and Ostertag R. 1983. The Ries impact crater. *Forschritte der Mineralogie* 61:71–116.

Sturkell E. F. F., Broman C., Forsberg P., and Torssander P. 1998. Impact-related hydrothermal activity in the Lockne impact structure, Jaemtland, Sweden. *European Journal of Mineralogy* 10:589–606.

Tugarinov A. I. and Naumov V. B. 1970. Decrepitation temperatures as influenced by the composition of gas-liquid inclusions and mineral strengths. *Doklady Akademii Nauk SSSR* 195:182–184.

Turtle E. P. and Pierazzo E. 1998. Constraints on the size of the Vredefort impact crater from numerical modeling. *Meteoritics & Planetary Science* 33:483–490.

Ulrich M. R. and Bodnar R. J. 1988. Systematics of stretching of fluid inclusions. II: Barite at 1 atm confining pressure. *Economic Geology and the Bulletin of the Society of Economic Geologists* 83:1037–1046.

Vityk M. O. and Bodnar R. J. 1995. Textural evolution of synthetic fluid inclusions in quartz during reequilibration, with applications to tectonic reconstruction. *Contributions to Mineralogy and Petrology* 121:309–323.

Vityk M. O., Bodnar R. J., and Doukhan J. 2000. Synthetic fluid inclusions: XV. TEM investigation of plastic flow associated with reequilibration of synthetic fluid inclusions in natural quartz. *Contributions to Mineralogy and Petrology* 139:285–297.

von Engelhart W. 1990. Distribution, petrography, and shock metamorphism of the ejecta of the Ries crater in Germany. *Tectonophysics* 171:259–273.

von Engelhardt W. 1997. Suevite breccia of the Ries impact crater, Germany: Petrography, chemistry, and shock metamorphism of crystalline rock clasts. *Meteoritics & Planetary Science* 32:545–554.

Warren P. H. Petrologic evidence for low-temperature, possibly flood evaporitic origin of carbonates in the ALH 84001 meteorite. *Journal of Geophysical Research* 103:16,759–16,773.

Whitehead J., Spray J. G., and Grieve R. A. F. 2002. Origin of "toasted" quartz in terrestrial impact structures. *Geology* 30: 431–434.

Zhang Y. 1998. Mechanical and phase equilibria in inclusion-host systems. *Earth and Planetary Science Letters* 157:209–222.

Zolensky M. and Barrett R. 1993. The genetic relationship between hydrous and anhydrous interplanetary dust particles. *Microbeam Analysis* 2:191–197.

Zolensky M. E., Bodnar R. J., Gibson E. K., Jr., Nyquist L. E., Reese Y., Shih C.-Y., and Wismann H. 1999. Asteroidal water within fluid inclusion-bearing halite in an H5 chondrite, Monahans. 1998. *Science* 285:1377–1379.

Zürcher L. and Kring D. A. 2004. Hydrothermal alteration in the core of the Yaxcopoil-1 borehole, Chicxulub impact structure, Mexico. *Meteoritics & Planetary Science* 39:1199–1221.